IEEE Access
Multidisciplinary | Rapid Review | Open Access Journal

Received September 16, 2019, accepted September 29, 2019, date of publication October 9, 2019, date of current version October 23, 2019.

Digital Object Identifier 10.1109/ACCESS.2019.2946443

Mine Fracturing Monitoring Analysis Based on High-Precision Distributed Wireless Microseismic Acquisition Station

SHUAIQING QIAO[1], QISHENG ZHANG[1], AND QIMAO ZHANG[2]
[1]School of Geophysics and Information Technology, China University of Geosciences (Beijing), Beijing 100083, China
[2]Institute of Electronics, Chinese Academy of Sciences, Beijing 100049, China

Corresponding author: Qisheng Zhang (zqs@cugb.edu.cn)

This work was supported in part by the Natural Science Foundation of China under Grant 41574131, in part by the National Key Research and Development Program of China under Grant 2017YFF0105704, in part by the National "863" Program of China under Grant 2012AA06110203, and in part by the Fundamental Research Funds for the Central Universities of China.

ABSTRACT A large number of shallow fossil fuel energy sources have been exhausted, including coal, oil, natural gas, and other non-renewable energy sources with rapid industrial development. The mining of fossil fuel energy has gradually shifted to the deep layers of the stratum, where safety is more difficult to guarantee. As a result, the development of a data acquisition system that can be used for microseismic monitoring and disaster prediction is imminent. In this study, in order to complete the design of a high-precision acquisition circuit, main control circuit, and other hardware circuits, the authors developed a set of high-precision distributed wireless microseismic acquisition stations, which was combined with three-component geophones to complete a microseismic monitoring system. This monitoring system was then verified through on-site work during the construction of a coal mine in China. This paper focuses on a detailed analysis of the data collected by the acquisition stations. Firstly, twelve sets of acquisition stations were used to conduct fixed-location blasting tests of the mine, which yielded good test results. Secondly, an analysis of microseismic monitoring data obtained during deep-well fracturing was carried out, and pre-fracturing static monitoring, carbon dioxide monitoring, fracturing monitoring, and post-fracturing static monitoring were also completed. This paper provides a detailed introduction to fracturing monitoring data of mines, combining discussions on the other three types of mine monitoring to reach relevant conclusions.

INDEX TERMS Acquisition station, fracturing monitoring, high-precision, microseismic, three-component.

I. INTRODUCTION

As an important basic energy source, coal plays a significant role in human production and life [1]. However, as a non-renewable energy source, most of the shallow coal resources in the world are gradually being exhausted, and coal mining is beginning to focus on those in the deeper layers of the stratum. As the risks due to coal-rock burst and mine pressure increase, coal mine disasters will become more common. As an important means of mine disaster prediction, distributed and networked seismic mine monitoring technology will become a trend [2], [3].

As a micro-fracture space monitoring technology, microseismic monitoring plays an important role in warning of rock rupture in underground engineering [4]. Microseismic monitoring first collects microseismic signals of rock rupture, then utilizes waveform analysis to obtain parameters such as the time, location, and source of the microseismic event [5]. By accurately determining the location of a microseismic event [6], it is possible to judge the spatial distribution of the rupture surface in the rock (fracture network) [7], [8]. Through the analysis of the development rate of a microseismic event or the evolution of source parameters in a certain area [9], [10], dynamic monitoring and early warning of rock burst disasters in tunnel boring can be realized [11]. Quantitative seismology can be used to analyse various types of mechanics information (such as seismic deformation, stress adjustment, stress release, etc.) of the rock rupture process [12], while microseismic monitoring and acquired parameters can identify the mechanical process of rock deformation and fracture [13].

The associate editor coordinating the review of this manuscript and approving it for publication was Jun Wu.

Dynamic properties of an elastic medium can be predicted by interpreting seismic research. Since anisotropy is related to the modelling problem of seismic wave propagation [14], [15], determining the original parameters of a seismic inversion is also affected by the anisotropy of the medium [16], [17]. In past research, a wealth of experience has been accumulated based on a large number of theoretical and algorithmic solutions for dynamic seismological problems [18], [19]. Seismology is a relatively common discipline in modern geophysics and plays a pivotal role in geological exploration and disaster prediction [20]–[22]. The main source of its data is seismic records of natural or man-made events on the Earth's surface, using existing acquired data to obtain characteristic information about the various aspects of wavefield propagation properties [23]. This paper proposes the use of near-surface geophysical techniques, which have been combined with geomorphological analysis to determine the natural subsurface processes acting on the study area [24].

However, the premise of all data analysis is the collection of microseismic data, and the quality of the collected data directly affects the credibility of subsequent data processing. At present, the instruments used for seismic monitoring have matured, with a variety of seismic monitoring instruments produced by established seismic instrument manufacturers, such as the 408UL, 428XL, and 508XT of SERCEL in France, and the G3iHD of INOVA; yet, instruments used specifically for microseismic monitoring are still immature [25]. In addition, their acquisition accuracy, synchronization accuracy, and real-time monitoring are lacking to different extents [26].

Furthermore, in the geophysical exploration industry, the development of exploration instruments and the analysis of geophysical data are often carried out separately, with little communication or cooperation between them. Therefore, in scientific research, it is vital to develop a microseismic acquisition and monitoring system for actual mine exploration.

II. DEVELOPMENT OF MICROSEISMIC ACQUISITION STATION AND ITS TECHNICAL INDICATORS

The overall development of the acquisition station includes the hardware circuit, operating program, and design of the mechanical structure. When using the acquisition station, the electrical engineer mainly considers its electrical performance. In field construction, however, the operational stability of the acquisition station appears especially important [27], because operational stability is the premise that the acquisition station can smoothly extract the microseismic signals in a harsh environment. Next, the electronic circuit design of the collection station will be described in detail.

A. HARDWARE CIRCUIT DESIGN

According to the development of seismic signals, the acquisition station can be roughly divided into three parts, as shown in Figure 1: 1) the high-sensitivity sensor, which converts the microseismic signal from the vibration signal into an electrical signal; 2) the acquisition circuit, which initially processes and converts the analogue electrical signal from the sensor into a digital electrical signal; 3) the control circuit, which stores the digital signal, uploads that signal to the upper computer, and controls the working state of the acquisition station, etc.

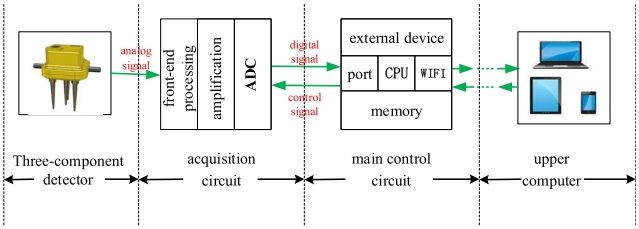

FIGURE 1. Overall block diagram of acquisition station.

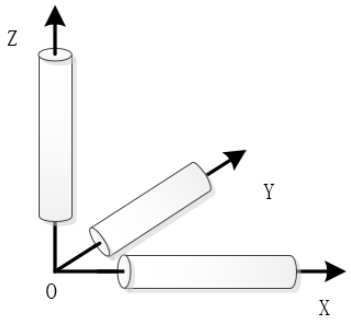

FIGURE 2. Three-dimensional map of geophone.

1) THREE-COMPONENT SENSOR

The sensor is the source of all geological detection instruments, and it is also an indispensable part. The intrinsic voltage sensitivity is 1.32 V / in./ sec.An electric acquisition instrument requires electrodes, a magnetic acquisition instrument requires a magnetic bar, and a logging instrument requires a series of sensors for temperature, pressure, and acceleration. Similarly, microseismic collectors require geophones. The three-component (3-C) geophone in this paper uses a traditional moving-coil vibration sensor, which uses the principle of electromagnetic induction to convert the input motion velocity into an inductive potential output in the coil. It directly converts the mechanical energy of the measured object into an electrical signal output. The geophone is a unit with three single-component sensors packaged together, as shown in Figure 2. As can be seen from this figure, the one-directional sensors are perpendicular to each other. The vibration signals (X component, Y component) in the horizontal direction and the vibration signal (Z component) in the vertical direction are respectively measured.

2) ACQUISITION CIRCUIT

The acquisition circuit plays a key role in the entire acquisition station because the signals in the whole system are input into the system from the acquisition circuit, which is the

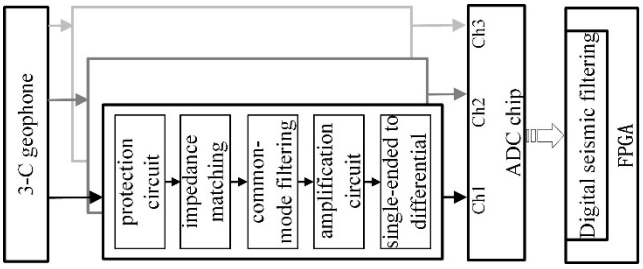

FIGURE 3. Structure diagram of acquisition circuit.

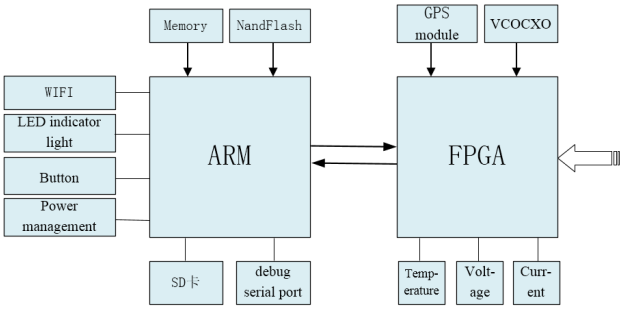

FIGURE 4. Main control circuit task-scheduling diagram.

source. As the quality of the signal is very important, noise processing is required. An indicator of the acquisition station, which is also mentioned below, the equivalent input noise is mainly determined by the acquisition circuit [28]. Figure 3 is a block diagram of the acquisition circuit. It can be seen from the figure that a part of the circuit's front end is a protection circuit, which mainly protects the subsequent circuit and prevents damage to other circuits due to destructive signals. An integral part of this protection circuit is the Schottky diode.

The second stage is impedance matching. This part of the circuit mainly matches the impedance with the internal impedance of the geophone to obtain a complete differential input signal. Since the seismic signal is a low frequency signal, while the signal input by the geophone is a differential signal, the input signal needs to be subjected to common mode filtering to filter out the high-frequency noise signal, and then the weak seismic signal needs to be amplified. In addition, since the output signal of the selected amplifier in the project is a single-ended signal, while the input of the analogue-to-digital conversion is a differential signal, the single-ended signal of the amplifier output needs to be converted into a differential signal. At the same time, further noise reduction is carried out, as well as input into the AD chip to convert the analogue signal into a digital signal so as to complete the acquisition process of the seismic signal [29].

3) MAIN CONTROL CIRCUIT

The main control circuit is the core of the distributed wireless microseismic acquisition station that allows all parts of the acquisition station to work in coordination. The part is responsible for not only pre-processing and storing data, but also a range of task-scheduling work. As shown in Figure 4, the control is accomplished through the GPIO port on the ARM processor in the main control circuit, achieving functions including control of power-on management, indicator lights, and buttons of the acquisition station. In addition, through the GPIO-extended Wi-Fi network of this processor, interaction and data transmission with the host computer are achieved.

In the main control unit, part of the task scheduling cannot be completed by the ARM core processor alone; therefore, in this paper, FPGA was used to assist the work. This work specifically includes the following: 1) acquisition station clock management, task scheduling and related strategy scheduling; 2) temporary buffering of data collected by the acquisition circuit; 3) uploading and processing information through GPS to allow synchronization across the acquisition station; 4) measurement of electrical parameters and ambient temperature during circuit operation; and 5) data communication.

TABLE 1. Performance indicators of acquisition station.

Item	Acquisition station indicator
Equivalent Input Noise (RMS)	0.50μV@40dB
Channel Crosstalk	108dB@4V&31.25HZ
Number of Channels	3
Data Transmission	Local Storage + Wireless Transmission
Maximum Input Signal	2.5 peak@0dB
Timing Accuracy	<100ns, GPS disciplined

B. KEY INDICATORS OF ACQUISITION STATION

After the hardware circuit of the acquisition station is developed, it is necessary to test the performance indicators of each aspect one by one, and then carry out the experimental verification. The detailed verification tests of the acquisition station are described in section 3, while this section mainly describes indicators such as equivalent input noise, synchronization accuracy, and the number of channels of the acquisition station. Table 1 shows the results of some of these indicators.

III. MICROSEIMIC DATA ACQUISITION AND PROCESSING ANALYSIS FROM ON-SITE DEEP WELL FRACTURING

A. PRELIMINARY INSTRUMENT TEST DATA ANALYSIS

After the development of the acquisition station was completed, it was necessary to test its actual applicability. This experiment used the method of drainage fixed-location blasting to test the acquisition station. The purpose of the experiment was to determine the location and range of influence of blasting. Monitoring was conducted through 16 distributed wireless microseismic acquisition stations developed in-house. GPS at the front-end of the distributed stations sampled and recorded data and analysed it after monitoring. The sampling bit depth was 24 bits, the dynamic range was

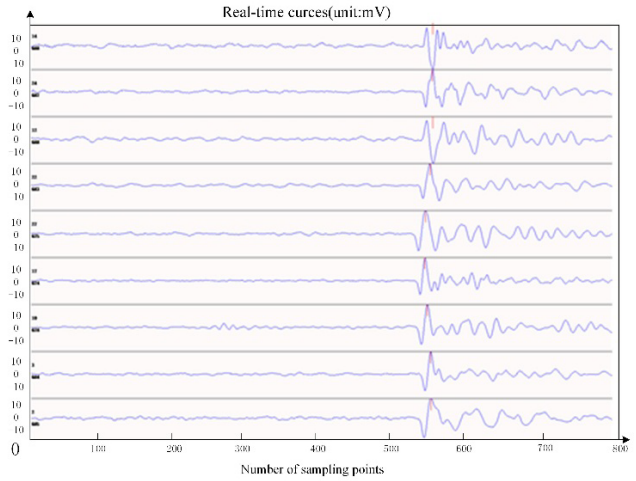

FIGURE 5. Blasting record waveform.

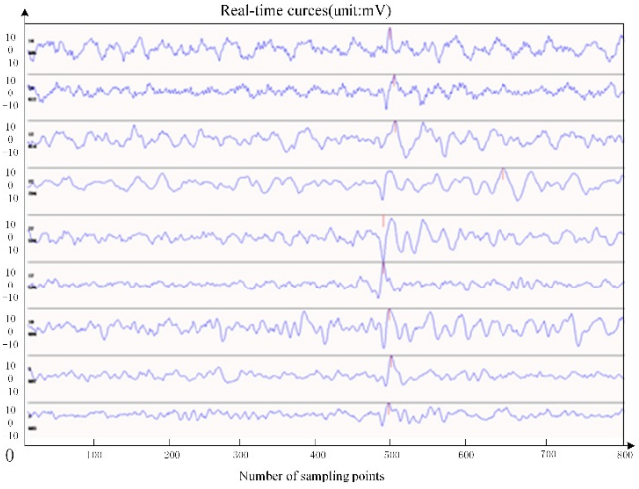

FIGURE 6. Blasting-induced microseismic waveform.

135db, and the sampling rate was 1000 Hz. Earthquakes of magnitude 0-2 could be recorded at the source.

In this case, the experimental site was randomly selected and implemented under the conditions of numerous uncertainties. Figure 5 and Figure 6 show the field test results. The results show that the data quality was good, and multiple clear microseismic waveforms can be seen (Figure 5, Figure 6).

It can be seen from Figure 5 and Figure 6 that when the amplitude of the blasting was at the maximum, the half period of the maximum amplitude reflected the source scale of the microseismic event. In addition, the microseismic event induced by the blasting had a small amplitude, with usually one to two large amplitudes, and the entire waveform envelope was in the shape of a swallow. Microseisms induced by other causes could be related to coal mine production, usually showing multiple peaks with similar amplitudes that appear continuously.

The location of the blasting source is denoted by the red circle in Figure 7, while the blue circles indicate the source

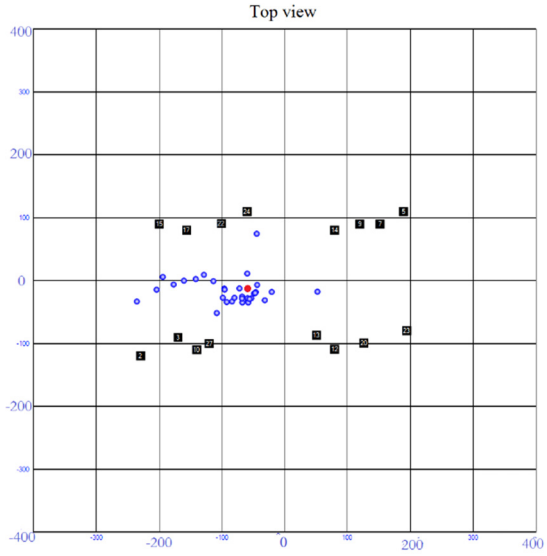

FIGURE 7. Microseismic source location distribution top view.

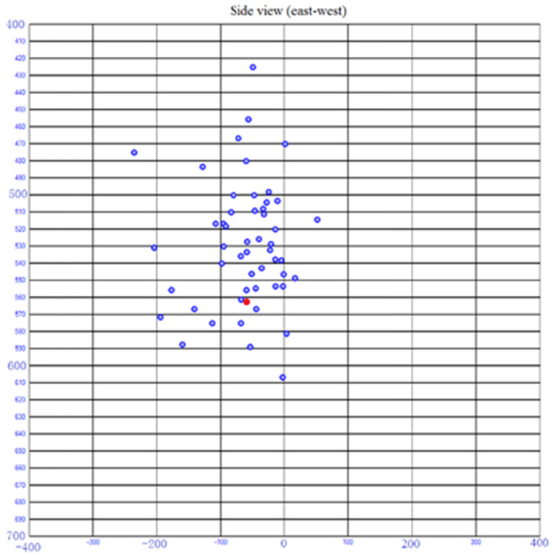

FIGURE 8. Side view of microseismic source locations in the east-west direction.

location of the induced microseismic events, and the black squares are the location of the acquisition stations. Along the east-west direction, the length of the affected area is approximately 60 m. Toward the west, a strip including scattered microseismic events with source points at different depths can be seen, which is about 100 m long. Along the north-south direction, the length of the affected area is approximately 50 m; in addition, scattered microseismic events can be seen in the far north. The near-field affected area can be judged as connected through fractures.

The location of the blasting source is shown by the red circles in Figure 5 and Figure 6, and the affected area is given by the induced secondary earthquakes. These secondary earthquakes, also known as microseismic events, have locations

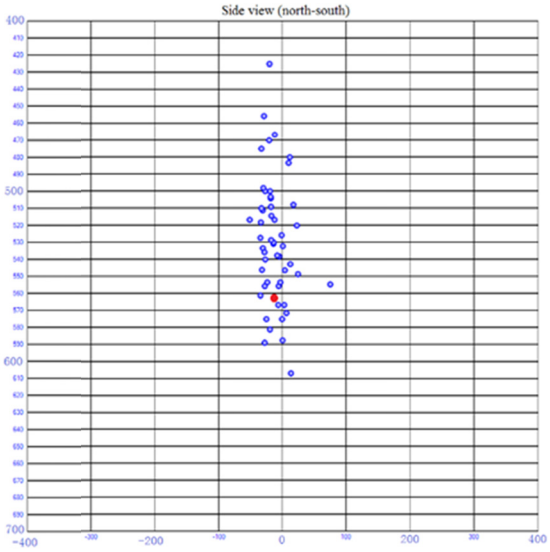

FIGURE 9. Side view of microseismic source locations in the east-west direction.

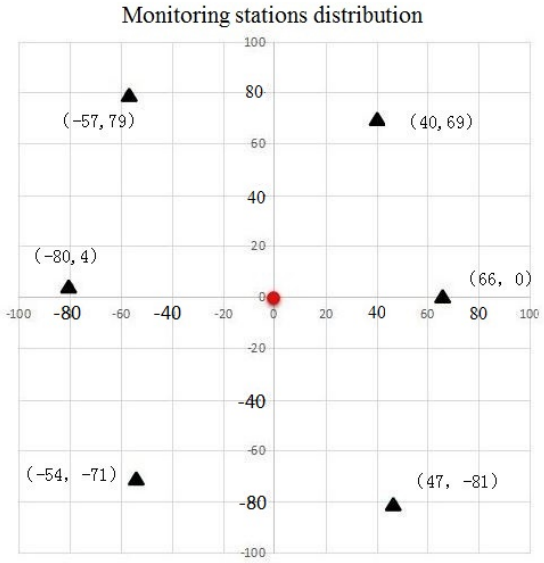

FIGURE 10. Deep well microseismic monitoring station distribution.

shown by the blue circles in Figure 8 and Figure 9. The blasting is equivalent to an earthquake of magnitude 0-0.2, and the average radius of the source is 16.2 m. In the depth direction, the affected area extends upwards to a large scale, while the directly-affected area has a scale of 60 m, where an interval seems to exist, which further extends upwards by 30 m.

From the test results, the actual location of the on-site drainage blasting is basically consistent with the location obtained by inversion of the data collected through the acquisition stations. It can be seen that the theoretical calculation results are accurate, and the data collected by the acquisition stations is stable and reliable and can be used in actual production.

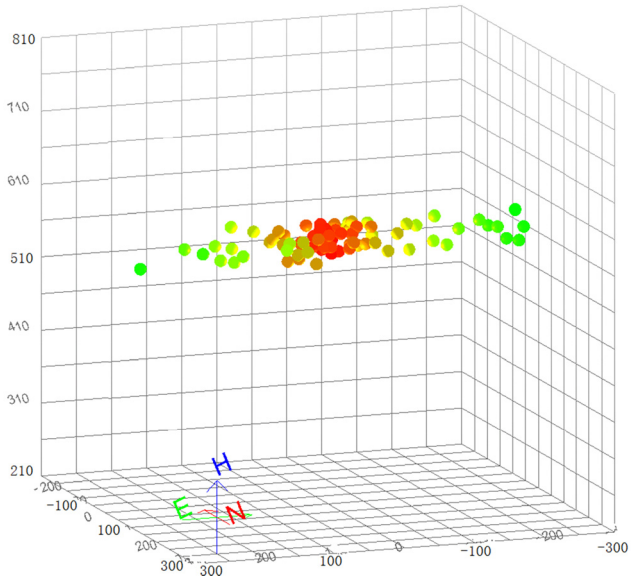

FIGURE 11. Fracturing monitoring 4D image.

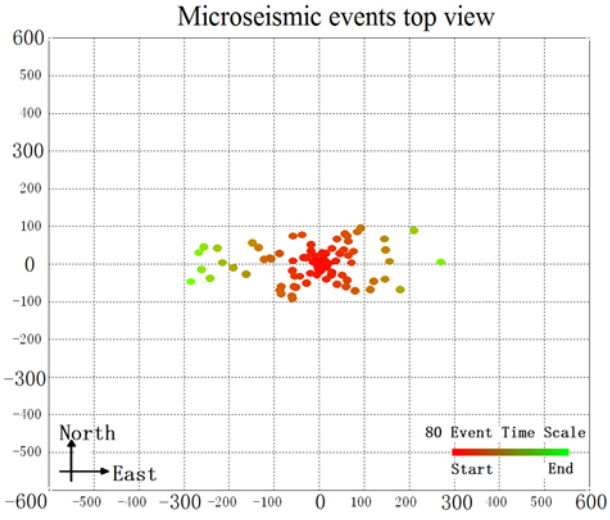

FIGURE 12. Fracturing monitoring top view.

B. ANALYSIS ANALYSIS OF DEEP WELL FRACTURING MICROSSEISMIC MONITORING DATA

Pre-fracturing static monitoring, carbon dioxide monitoring, fracturing monitoring, and post-fracturing static monitoring were carried out on this well. The monitoring interval was 506.70-514.50 m, and the vertical depth was 510.6 m. During operation, fractures occurred along the original crack in the earth layer, and the increase in gap pressure also caused cracks and faults, thus inducing microseismic events. The pre-fracturing monitoring time was 120 minutes, the fracturing monitoring time was 150 minutes, and the post-press monitoring time was 120 minutes.

By identifying and locating microseismic events, the location, size, and extent of these microseismic events were inversed. The monitoring results show that the average

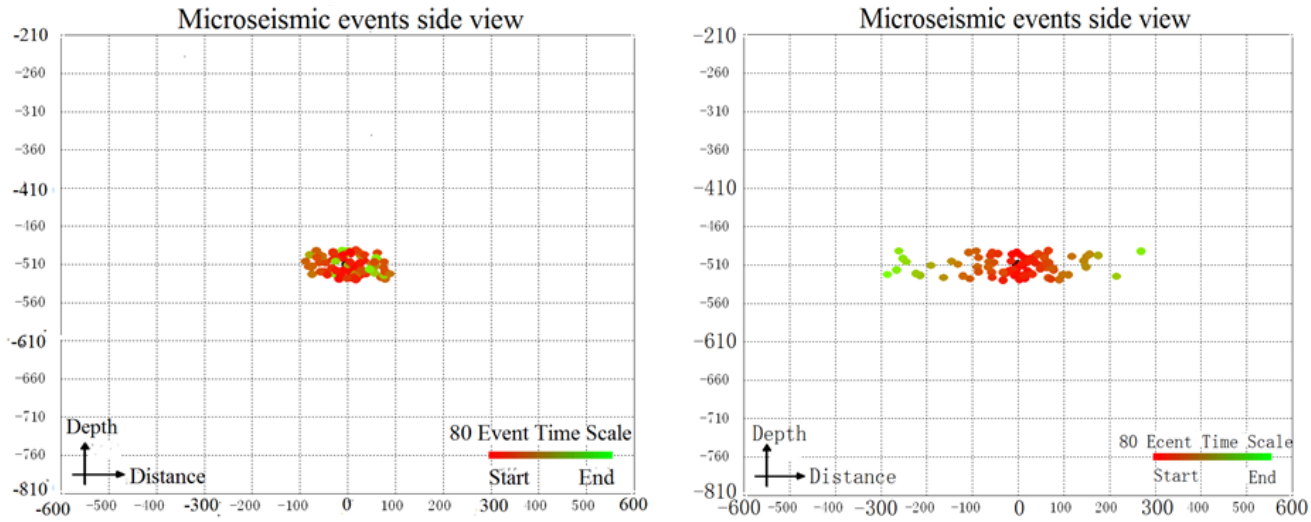

FIGURE 13. (a) Fracturing monitoring side view (parallel to fracture direction). (b) Fracturing monitoring side view (perpendicular to fracture direction).

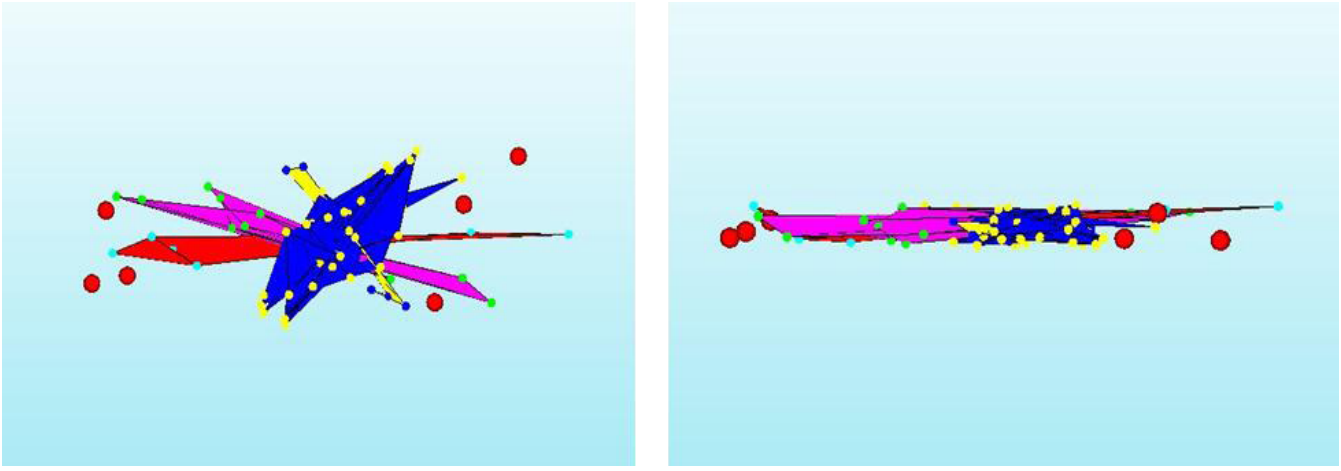

(a) Fracturing monitoring 3D image top view.

(b) Fracturing monitoring 3D image side view

FIGURE 14. (a) Fracturing monitoring 3D image top view. (b) Fracturing monitoring 3D image side view.

fracture direction of the pre-fracturing static monitoring of the XX well was 73.9 degrees northeast, 76.9 degrees northeast for carbon dioxide monitoring, 87.4 degrees northeast for fracturing monitoring, and 79.3 degrees northeast for post-fracturing static monitoring.

1) PRELIMINARY PREPARATION

The project used a planar microseismic network, and Figure 10 shows an example of a 6-station planar microseismic network, using wireless transmission. The coordinates in the figure were determined using the projection of the operation layer on the ground as the origin of the coordinate system. The horizontal axis is along the east-west direction with east as positive; the vertical axis is along the north-south direction with north as positive. The red circle in the figure indicates the projection of the operation layer on the ground, and the black triangles represent the locations of the geophones.

2) FRACTURING MONITORING RESULTS

The monitoring depth was 506.70-514.50 m, while the vertical depth was 510.6 m. The location of each source point can be clearly seen from the four-dimensional view shown in Figure 11. Combining all source points, the direction and height of the fracture propagation is indicated [30,31], and the colour indicates the time sequence of the microseismic occurrence. By projecting the 4D image on a plane, a top view and a side view of the source locations can be obtained, as shown in Figure 12 and Figure 13(a)(b).

The upper and lower limits of the fracturing monitoring depth and the height range of the monitoring section can be seen from the parameter table of Table 2. This depth range is the result of direct computer calculations and can be compared to the given depth range.

The top view (Figure 12) shows that as the well underwent fracturing, many artificially-created parallel fractures

TABLE 2. Fracturing monitoring parameters.

Fracture geometric parameters（Height /m）			
Upper limit:	491.08	Variance:	11.53
Lower limit:	530.12	Variance:	11.59
Height difference:	39.04	Variance:	11.56

TABLE 3. Artificial fracture parameters and influent fracture scale.

Session	West-wing influent fracture length (m)	East-wing influent fracture length (m)	Influent fracture height (m)
Value at 75% Confidence	212.5	231.0	33
Variance (%)	12.93	10.17	11.55

and oblique fractures were formed in the north-east direction. The side view (Figure 13(a)(b)) perpendicular to the fracture direction indicates the generally stable fracture height and its variation with length. From the results, it can be derived that the fractures developed asymmetrically on the two sides of the well. The reason for this asymmetry was usually caused by the complexity of the stratigraphic structure and lithology, as well as the difference in permeability.

As can be seen from Figure 14(a)(b), the main seam (blue) was 40 degrees northeast, with three distinct sub-cracks in directions of 35 degrees northwest, 75 degrees northwest, and near east-west. Figure 15 above shows the possible fractures. It can be seen from the figure that the development of primeval fractures in the near-well induced by the leakage of fracturing fluid were 50-80 degrees northeast and 10-40 degrees northwest. The figure shows the existence and orientation of non-structural cracks.

3) MONITORING ERROR ANALYSIS

According to the calculation principle of error analysis, the calculation error of the distance d between two different microseismic points is

$$E^*(d) = \frac{v_p^* \Delta^* t}{L^*}(E^*(v_p) + E^*(\Delta t)) \tag{3-1}$$

The error of Δt in Equation 3-1 generally depends on the scale error of the first-time reading. When the sampling interval of the microseismic recording is 1ms, the relative error ofΔt is 1% - 5%. The precision of velocity, $E^*(v_p)$, depends on the quality of the original data and the calculation method of velocity, which is about 2% - 6%. Due to the approximation of $L^* = v_p^* \Delta^* t L^* = v_p^* \Delta^* t$, the precision of $E^*(d)$ is in the range of 3% - 11%. Considering that the source-velocity joint inversion can achieve a higher precision, the actual error range should be less than 10%.

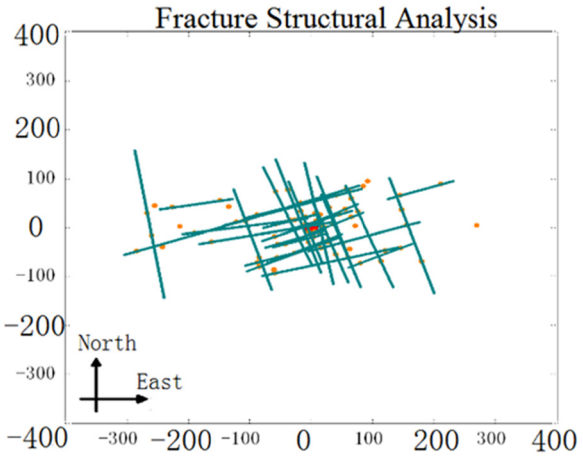

FIGURE 15. Fracturing monitored primeval fracture orientation induced by fracturing fluid leakage.

Here, we use the normal distribution theory to analyse the scale measurement error by the T test method. The confidence of the T test is set to 0.75, and the scale error can be calculated by the T distribution table and Equation 3-2 to Equation 3-5 [32,33].

$$\overline{X} = \sum_{i=1}^{n} \frac{X_i}{n} \tag{3-2}$$

$$S^2 = \sum_{i=1}^{n} \frac{(X_i - \overline{X})^2}{n-1} \tag{3-3}$$

$$D_{0.75} = t \times S \div \sqrt{n} \tag{3-4}$$

$$D'_{0.75} = \frac{D_{0.75}}{D_{0.75} + \overline{X}} \tag{3-5}$$

where n is the sample number of microseismic points, $\overline{X}$ and S represent the sample mean and unbiased estimator of variance, $D_{0.75}$ indicates the absolute error when the confidence is 75%, $D'_{0.75}$ indicates the relative error when the confidence is 75%, and t indicates the value of the T-distribution table when the confidence is 75%.

4) FRACTURING MONITORING SUMMARY

Due to crack tip effects [34], [35], the actual influent fracture size was smaller than the monitoring scale. Table 3 lists the artificial fracture parameters and the influent fracture scale at 75% confidence.

1. The trend in orientation of artificial fractures in hydraulic fracturing was 87.4 degrees northeast and the total length of fractures was 443.5 m (Table 4).
2. The length of influent fractures in the west wing of the hydraulic fracturing was 212.5 m, and the length of influent fractures in the east wing was 231.0 m. The height of influent fractures was 33 m.
3. The near-well primeval fractures were moderately developed, ranging from 50-80 degrees in the northeast and 10-40 degrees in the northwest. The inclination angle was 1 degree, and the average fracture surface tended to the southeast.

TABLE 4. Artificial fracture orientation.

Satistical Orientation (°)	Inclination (°)	Trend	Main Fracture Trend (°)	Sub-fracture Trend (°)
Northeast 87.4	1	Southeast	Northeast 40	Northwest 35, Northwest 75, Near East-west

IV. CONCLUSION

In order to alleviate the safety problems in mineral mining, a distributed wireless microseismic acquisition system for mine monitoring is developed in this paper. The paper briefly introduces the hardware development principle and the electrical indicators of acquisition stations. Based on this self-developed microseismic acquisition system, a preliminary test and a later practical application were carried out in a mine in China. The data obtained from the microseismic acquisition system were processed and analysed in detail. In consideration of actual coal mining operations, the results show that this acquisition system is very successful for fracturing monitoring applications and can be applied to the safety monitoring of actual mining activities.

REFERENCES

[1] S. Dai and R. B. Finkelman, "Coal geology in China: An overview," *Int. Geol. Rev.*, vol. 60, nos. 5–6, pp. 531–534, Nov. 2017.
[2] G. Li, J. Wu, J. Li, K. Wang, and T. Ye, "Service popularity-based smart resources partitioning for fog computing-enabled industrial Internet of things," *IEEE Trans. Ind. Informat.*, vol. 14, no. 10, pp. 4702–4711, Oct. 2018.
[3] S. J. Gibowicz, "Seismicity induced by mining," *Adv. Geophys.*, vol. 51, pp. 1–53, Jan. 2009.
[4] R. Govers, K. P. Furlong, L. van de Wiel, M. W. Herman, and T. Broerse, "The geodetic signature of the earthquake cycle at subduction zones: Model constraints on the deep processes," *Rev. Geophys.*, vol. 56, no. 1, pp. 6–49, Mar. 2018.
[5] L. Shu, M. Mukherjee, and L. Hu, "Geographic routing in duty-cycled industrial wireless sensor networks with radio irregularity," *IEEE Access*, vol. 4, pp. 9043–9052, 2016.
[6] G. Kwiatek, "Relative source time functions of seismic events at the Rudna copper mine, Poland: Estimation of inversion uncertainties," *J. Seismol.*, vol. 12, no. 4, pp. 499–517, Oct. 2008.
[7] X. Lin, J. Li, J. Wu, H. Liang, and W. Yang, "Making knowledge tradable in edge-AI enabled IoT: A consortium blockchain-based efficient and incentive approach," *IEEE Trans. Ind. Informat.*, to be published. doi: 10.1109/TII.2019.2917307.
[8] J. Wu, M. Dong, K. Ota, J. Li, W. Yang, and M. Wang, "Fog-computing-enabled cognitive network function virtualization for an information-centric future Internet," *IEEE Commun. Mag.*, vol. 57, no. 7, pp. 48–54, Jul. 2019.
[9] J. Wu, M. Dong, K. Ota, J. Li, and Z. Guan, "FCSS: Fog computing based content-aware filtering for security services in information centric social networks," *IEEE Trans. Emerg. Topics Comput.*, to be published. doi: 10.1109/TETC.2017.2747158.
[10] Y. Kaneko and P. M. Shearer, "Variability of seismic source spectra, estimated stress drop, and radiated energy, derived from cohesive-zone models of symmetrical and asymmetrical circular and elliptical ruptures," *J. Geophys. Res.*, vol. 120, no. 2, pp. 1053–1079, Feb. 2015.
[11] C.-P. Lu, G.-J. Liu, and Y. Liu, "Microseismic multi-parameter characteristics of rockburst hazard induced by hard roof fall and high stress concentration," *Int. J. Rock Mech. Mining Sci.*, vol. 76, no. 6, pp. 18–32, Jun. 2015.
[12] F. Mulargia, S. Castellaro, and M. Ciccotti, "Earthquakes as three stage processes," *Geophys. J. Int.*, vol. 158, no. 1, pp. 98–108, Jul. 2004.
[13] S. Amini and P. P. Valkó, "Using distributed volumetric sources to predict production from multiple-fractured horizontal wells under non-darcy-flow conditions," *SPE J.*, vol. 15, no. 1, pp. 105–115, Mar. 2010.
[14] T. Alkhalifah and R. É. Plessix, "A recipe for practical full-waveform inversion in anisotropic media: An analytical parameter resolution study," *Geophysics*, vol. 79, pp. 91–101, Mar. 2014.
[15] I. Tsvankin, J. Gaiser, V. Grechka, M. Van Der Baan, and L. Thomsen, "Seismic anisotropy in exploration and reservoir characterization: An overview," *Geophysics*, vol. 75, no. 5, pp. 15–29, Sep. 2010.
[16] E. A. Alwan, S. B. Venkatakrishnan, A. A. Akhiyat, W. Khalil, and J. L. Volakis, "Phase error evaluation in a two-path receiver front-end with on-site coding," *IEEE Access*, vol. 3, pp. 55–63, 2015.
[17] G. A. Meles, J. Van der Kruk, S. A. Greenhalgh, J. R. Ernst, H. Maurer, and S. A. Greenhalgh, "A new vector waveform inversion algorithm for simultaneous updating of conductivity and permittivity parameters from combination crosshole/borehole-to-surface GPR data," *IEEE Trans. Geosci. Remote Sens.*, vol. 48, no. 9, pp. 3391–3407, Sep. 2010.
[18] P. Lan, K. Polychronopoulou, L. Iaccino, X. Bao, and A. Polycarpou, "Elevated-temperature and-pressure tribology of drilling fluids used in oil and gas extended-reach-drilling applications," *SPE J.*, vol. 23, no. 6, pp. 2339–2350, Aug. 2018.
[19] S. Khan and R. Guida, "Application of mellin-kind statistics to polarimetric *G* distribution for SAR data," *IEEE Trans. Geosci. Remote Sens.*, vol. 52, no. 6, pp. 3513–3528, Jun. 2014.
[20] J. Wu, M. Dong, K. Ota, J. Li, and Z. Guan, "Big data analysis-based secure cluster management for optimized control plane in software-defined networks," *IEEE Trans. Netw. Service Manage.*, vol. 15, no. 1, pp. 27–38, Mar. 2018.
[21] H.-Z. Yu, J. Cheng, X.-T. Zhang, L.-P. Zhang, J. Liu, and Y.-X. Zhang, "Multi-methods combined analysis of future earthquake potential," *Pure Appl. Geophys.*, vol. 170, nos. 1–2, pp. 173–183, Jan. 2013.
[22] V. Keilis-Borok, P. Shebalin, A. Gabrielov, and D. Turcotte, "Reverse tracing of short-term earthquake precursors," *Phys. Earth Planet. Interiors*, vol. 145, nos. 1–4, pp. 75–85. Jul. 2004.
[23] A. Pavlova, O. Hrytsai, and D. Malytskyy, "Determining the focal mechanisms of the events in the carpathian region of Ukraine," *Geosci. Instrum. Methods Data Syst.*, vol. 3, no. 2, pp. 109–164. 2014.
[24] M. A. Lazzari, A. Loperte, and A. Perrone, "Near surface geophysics techniques and geomorphological approach to reconstruct the hazard cave map in historical and urban areas," *Adv. Geosci.*, vol. 24, pp. 35–44, Mar. 2010.
[25] Z. Qi-Sheng, D. Ming, G. Jian, L. Wei-Bing, W. Qi, and F. Yong-Qiang, "Development of a new seismic-data acquisition station based on system-on-a-programmable-chip technology," *Ann. Geophys.*, vol. 56, no. 3, p. 0329, Aug. 2013.
[26] M. Peng, L. Yang, J. Zhang, T. Chen, U. Celentano, J. Röning, N. Y. Ermolova, and O. Tirkkonen, "IEEE access special section editorial: Recent advances in cloud radio access networks," *IEEE Access*, vol. 2, pp. 1683–1685. 2014.
[27] A. J. Mendecki, R. A. Lynch, and D. A. Malovichko, "Routine microseismic monitoring in mines," in *Proc. Austral. Earthq. Eng. Soc., Annu. Conf. Perth*, Nov. 2010, pp. 1–33.
[28] Q. Zhang*, J. Jiang, J. Zhai, X. Zhang, Y. Yuan, and X. Huang, "Seismic random noise attenuation using modified wavelet thresholding," *Ann. Geophys.*, vol. 59, no. 6, p. 0647, Jan. 2016.
[29] M. Kahrs, "50 years of RF and microwave sampling," *IEEE Trans. Microw. Theory Techn.*, vol. 51, no. 6, pp. 1787–1805, Jun. 2003.
[30] Y. Ben-Zion and V. Lyakhovsky, "Accelerated seismic release and related aspects of seismicity patterns on earthquake faults," *Pure Appl. Geophys.*, vol. 159, no. 10, pp. 2385–2412, Aug. 2002.
[31] S. C. Jaume and L. R. Sykes, "Evolution toward a critical point: A review of accelerating seismic moment/energy release prior to large great earthquakes," *Pure Appl. Geophys.*, vol. 155, nos. 2–4, pp. 279–305, 1999.

[32] G. Vasile, F. Pascal, J. P. Ovarlez, P. Formont, and M. Gay, "Optimal parameter estimation in heterogeneous clutter for high-resolution polarimetric SAR data," *IEEE Geosci. Remote Sens. Lett.*, vol. 8, no. 6, pp. 1046–1050, Nov. 2011.
[33] M. Wang, S. Yang, Z. Liu, and Z. Li, "Collaborative compressive radar imaging with saliency priors," *IEEE Trans. Geosci. Remote Sens.*, vol. 57, no. 3, pp. 1245–1255, Mar. 2019.
[34] J. P. Castagna, M. L. Batzle, and R. L. Eastwood, "Relationships between compressional-wave and shear-wave velocities in clastic silicate rocks," *Geophysics*, vol. 50, no. 4, pp. 571–581, Apr. 1985.
[35] C. Liu, Y. Liu, X. Feng, and Y. Lu, "Constructing the convex quadratic function for the evaluation of crack density of HTI media using P-and converted waves," *J. Geophys. Eng.*, vol. 9, no. 6, pp. 729–736, Nov. 2012.

SHUAIQING QIAO was born in Shanxi, China, in 1993. He received the B.E. degree in measurement and control technology and instrumentation from the China University of Geosciences (Beijing), in 2017, where he is currently pursuing the Ph.D. degree. His main research interest includes the instrument science and technology.

QISHENG ZHANG was born in Anhui, China, in 1978. He received the M.S. and Ph.D. degrees from the Geosciences University of China, Beijing, China, in 2012.

He has been with the School of Geophysics and Information Technology, China University of Geosciences, Beijing, since 2005. He is currently an Associate Professor with the School of Geophysics and Information Technology. His research interests include system-on-a-programmable-chip technology, measurement technology and instrument, high precision data-converters, and geophysical instruments.

QIMAO ZHANG was born in Anhui, China, in 1987. He received the M.Sc. degree from the Geosciences University of China, Beijing, China, in 2012. He is currently a Research Assistant with the Institute of Electronics of the Chinese Academy of Sciences (IECAS), Beijing.